

# A Study on Slot Leakage Inductance Considering the Saturation of WFSM for Electric Vehicles

Cheon-Ho Song<sup>1</sup>, Byeong-Chul Lee<sup>2</sup>, Ki-Chan Kim<sup>\*3</sup>

<sup>1,2</sup>Master degree, Dept. of Electrical Eng., Hanbat National Univ., Daejeon 34158, Republic of Korea

<sup>\*3</sup>Professor, Dept. of Electrical Eng., Hanbat National Univ., Daejeon 34158, Republic of Korea  
dlzk@naver.com<sup>1</sup>, soonia0000@naver.com<sup>2</sup>, kckim@hanbat.ac.kr<sup>\*3</sup>

## Article Info

Volume 83

Page Number: 4126 - 4134

Publication Issue:

March - April 2020

## Article History

Article Received: 24 July 2019

Revised: 12 September 2019

Accepted: 15 February 2020

Publication: 26 March 2020

## Abstract

The leakage magnetic flux in the motor is an unnecessary parameter that does not affect the generation of torque. Although there is a formula for calculating the inductance due to the leakage magnetic flux, there is a difference between the formula and the actual measured value because it is difficult to consider the saturation phenomenon of the stator core generated in the motor. In the case of WFSM, the field flux changes according to the field current, so the entire flux flowing through the stator core changes. These factors make the difference between the value obtained from the theoretical calculation of the leakage inductance and the actual measured leakage inductance value. In this paper, the effects of core saturation and field current on leakage inductance are analyzed. Based on the analyzed data, we derived the equation considering the saturation and the field current from the existing leakage inductance formula. Newly derived formulas analyze the effects of field current and saturation on leakage inductance.

**Keywords:** WFSM, Leakage inductance, Field current, Saturation

## 1. Introduction

As carbon emission is a global issue, electric vehicles (EVs) are being developed to replace fuel engine vehicles in many countries. As EVs use batteries rather than coal fuel, they can be driven without carbon emission. EVs run on electricity, and as such, they use motors instead of engines. Most of the existing traction motors are interior permanent magnet synchronous motors (IPMSMs) using rare earth materials, whose prices have increased owing to the increasing demand for EVs. The wound field synchronous motor (WFSM) is emerging as a substitute for IPMSM because of the high price of rare earth magnets. The wound field rotor creates magnetic flux through the excited winding instead of a permanent magnet.

WFSM has some features that make it different from IPMSM. For one, in WFSM, additional

copper loss occurs during the rotor winding because it uses winding instead of a permanent magnet. Therefore, it has worse efficiency. In other respects, WFSM has a salient structure while IPMSM has a reverse salient structure. Therefore, in WFSM, the maximum torque point occurs when the current angle is negative. When the value of the field current increases, the maximum torque point may appear at a value larger than the current 0° angle. Therefore, the characteristics of the motor depend on the field current, and as such, it is important to select the appropriate field current. The other difference is field current control.

As IPMSM cannot control the magnetic flux of the permanent magnet, it uses the field weakening method to flow a negative d-axis current. WFSM can also use field weakening control. Additionally, WFSM diminishes the rotor magnet flux by

changing the rotor winding current. Therefore, WFSM can drive more efficiently. Optimal design techniques are required, however, to achieve high efficiency. There are many optimal designs of WFSM [1]-[4].

The leakage magnetic flux flowing in the slot in the motor is a component that does not generate torque, but it is difficult to accurately calculate the leakage flux due to the saturation of the motor [5]-[8]. It is hard to predict because saturation is nonlinear. Almost all equations of leakage inductance express permeance, without saturation [9]-[11]. The effect of field flux is also not included in the leakage inductance equation. It should be considered because leakage flux is sensitive to flux in the stator core.

In this paper, the two-dimensional finite element method (2D-FEM) was used to analyze the effects of the saturation phenomenon and flux due to the field current on the slot leakage inductance. The slot leakage inductance obtained via 2D-FEM is compared with the leakage inductance obtained using the known leakage inductance formula [12]-[13]. Moreover, the change of the saturation and the flux of the field is digitized and substituted into the equation to prove the result.

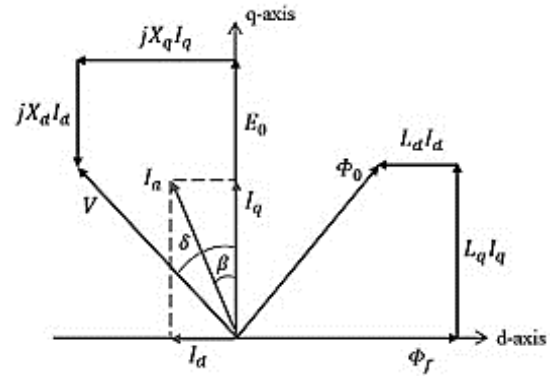


Figure 1. Vector diagram in the dq-axis

## 2. Basic Theory and Analysis Model of WFSM

### 2.1 Characteristics of WFSM

WFSM has a salient structure in the shape of a rotor. Thus, as the rotor rotates, the reluctance in the airgap changes. In the case of a motor with such a salient structure, the part with the smallest reluctance in the airgap is set as the d-axis, and the part with a phase difference of 90 electrical degrees with respect to the d-axis is set as the q-axis. As the magnetic flux moves in the direction with the smallest reluctance, the field flux is aligned on the d-axis. When current is applied to the armature winding, the armature magnetic flux affects the field magnetic flux. The influence of the armature magnetic flux is expressed by the product of the current and inductance. Figure 1 shows a vector diagram of WFSM in the dq-axis. The armature current was divided by the dq-axis. The angle between the armature current and the q-axis is called “ $\beta$ .” In almost all WFSMs, the maximum torque occurs in the first quadrant, but if the field current is large, the driving region is set in the second quadrant. As the rotor rotates, the inductance becomes a reactance component, which causes a reactance voltage drop. This voltage drop is expressed as the equations below.

$$V_q = X_d I_d + X_{ad} I_f (= E_0)$$

$$V_d = X_q I_q$$

$$V = E_0 + jX_d I_d + jX_q I_q \quad (1)$$

The dq-axis reactance includes the leakage reactance due to the leakage magnetic flux generated in the magnetic path. The reactance equation, including the leakage reactance, is as shown below.

$$X_d = X_{ds} + X_l$$

$$X_q = X_{qs} + X_l \quad (2)$$

As WFSM is a salient structure, there is a reluctance torque due to the reluctance difference in the dq-axis. In addition, there is a magnetic torque generated by the field and armature fluxes, which is proportional to the field and armature currents. The total torque is expressed as shown below.

$$T = \frac{1}{\omega} [X_{ad} I_f I_a \cos \beta + \frac{1}{2} (X_{ds} - X_{qs}) I_a^2 \sin 2\beta] \quad (3)$$

In equation (3), the first term is the magnetic torque, and the second term is the reluctance torque. As can be seen in equations (2) and (3), the leakage reactance not only has no effect on the torque but also has a negative effect on the power factor. The leakage flux is calculated using the formula utilizing permeance because the leakage magnetic flux is determined according to the structure of the slot.

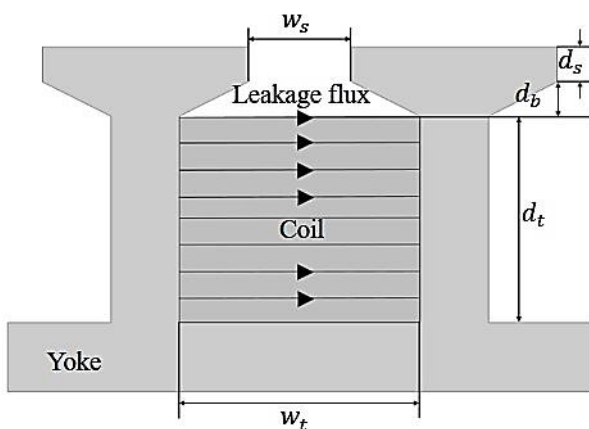


**Figure 2. Slot model for the calculation of the leakage inductance**

## 2.2 Theoretical calculation of the slot leakage inductance

Figure 2 shows a slot model for the calculation of the leakage inductance. It shows the leakage flux between two teeth. The coil lies in the entering direction in the slot, and the leakage flux flows from the left to the right tooth. Its magnetic field follows the righthand rule. The inductance is proportional to the permeance, and this permeance is due to the structure of the slot. There are parameters for the calculation of the permeance in Figure 3. The slot can be divided into three parts: the tooth, bend, and shoe parts. First, the permeance calculation at the tooth part differs from those in the other parts because this part includes conductors, causing disturbance of the leakage flux. Considering the disturbing magnetic flux component, the effective permeance is one-third of the previous permeance of the tooth part. As there is no disturbance of the leakage magnetic flux by the coil except for this part, the permeance can be calculated by the area and length of the magnetic path. In Figure 2,  $d$  means the distance of each part, and  $w$  means the width of the slot. In the case of the bend, as the widths of the upper and lower parts of the bend region are different, the permeance is obtained as the average of the two values. The slot leakage inductance can be obtained by determining the permeance through the above values and multiplying the square of the number of turns per coil. The equation of inductance is expressed as shown below.

$$L_s = N^2 \mu_0 L_{st} \left[ \frac{d_t}{3w_t} + \frac{d_b}{(w_t + w_s)/2} + \frac{d_s}{w_s} \right] \quad (4)$$

From equation (4), it can be seen that the leakage flux is large at the part where the coil is not wound, and the leakage is large at the shoe where the slot width is narrow.

### 2.3 Analysis model of WFSM

Figure 3 shows the basic analysis model. It has 8 poles and 48 slots as shown in table 8. The winding layout is a single layer. The number of series turns is 18, and the number of parallel branches is four. As this motor is designed for EVs, it has high power capability. Its power is 80 kW. Its field current is high to satisfy the required torque and power. It is a high-power, high-efficiency model with a shaft-cooling-type motor, although it has large copper loss caused by the field current, through the use of a high field current. Due to this characteristic, unlike the typical WFSM model, the maximum torque appears when the current phase angle is in the second quadrant. The base speed of this model is 3000 rpm, and the maximum torque generated is 255 Nm.

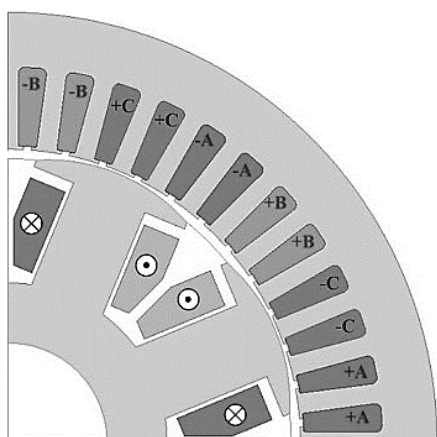


Figure 3. WFSM basic model

Table 1 : Specifications of the basic model

Parameter	Value	Unit
Number of poles	8	-
Number of slots	48	-
Outer diameter	200	mm
Stack length	190	mm
Power	80	kW
Rated torque	255	Nm
Rated speed	3000	rpm
Field Current	12	A <sub>dc</sub>

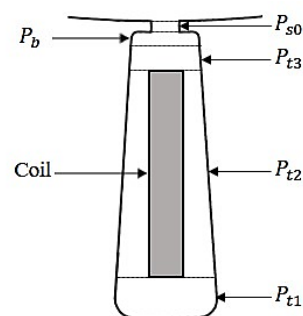


Figure 4. Permeance measurement points

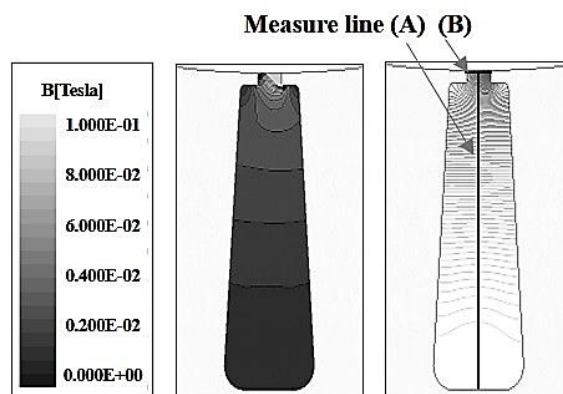
### 3. Comparison of Leakage Inductance Values

#### 3.1 Theoretical calculation of the leakage inductance

Figure 4 shows the slot of the FEM model divided into five permeance parts. For a more accurate calculation of the leakage inductance, the actual slot shape was subdivided by permeance. P\_t2 is applied with the efficient permeance applied in the above equation because there are conductors generating disturbing flux. The FEM model slot leakage inductance equation is expressed as shown below.

$$L_s = N^2 \mu_0 L_{st} [P_s + P_b + P_{t1} + \frac{P_{t2}}{3} + P_{t3}] \quad (5)$$

The length and width of each part were measured, and the permeance was calculated. The tooth part was expressed by segmenting the parts with and without the coil.



(a) leakage flux density (b) leakage flux line

Figure 5. FEM slot model for the measurement of leakage inductance

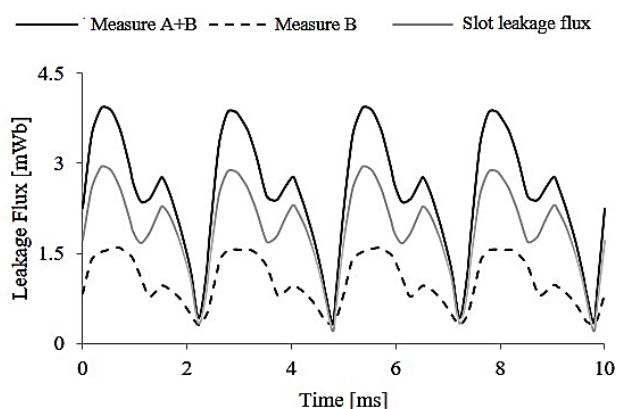


**Figure 6. Measured slot leakage flux by using measure line**

### 3.2 Measurement of the slot leakage inductance using FEM

Figure 5(a) shows the distribution of the magnetic flux density, and Figure 5(b) shows the magnetic flux. Two measuring lines were drawn to accurately measure the magnetic flux flowing through the teeth in the slot. Each measurement line measures the magnetic flux passing through the corresponding line. If only measurement line (A) exists, it will measure not only the leakage flux but also the flux linking from the field to the tooth side. Therefore, measurement line (B) serves to filter the magnetic flux that flows out of the field. To measure the exact leakage flux, the flux passing through measurement line (B) is removed from the flux passing through the measurement line that unites (A) and (B). Figure 6 shows the results of the above process.

**Table 2 : Comparison of the slot leakage inductance values**

Ia	Slot leakage inductance						Unit
	50	100	150	200	250	300	
FEM	71.0	51.3	46.4	44.4	43.3	42.4	$\mu\text{H}$
Calculation	42.04						

Table 2 shows the values obtained when the leakage inductance is measured via FEM and when it is calculated via theoretical calculation. The above data recorded the leakage inductance

through FEM measurements as armature current changes when the field current was 12 A. The inductance obtained via theoretical calculation had a constant value regardless of the armature current, but differed from the result obtained via FEM.

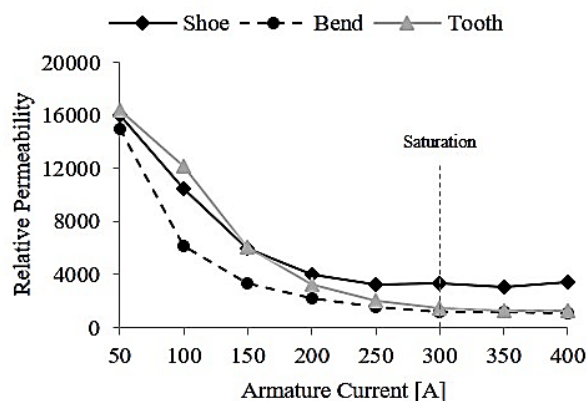


**Figure 7. Graph of relative permeability according to the armature current**

### 4. Analysis of the Saturation and Field Current

The motor generates torque through the interaction of the field and armature fluxes. The traction motor for an EV requires a large torque, and as such, a high value of the current for generating a magnetic flux is required. As the core of the motor is made up of a ferromagnetic material, the saturation has the characteristic of decreasing the relative permeability as the magnetic flux amount is increased. Not only the saturation but also the increase of the leakage magnetic flux by the field magnetic flux cannot be ignored. As the output of the motor is large, the magnetic flux flowing through the armature core is greatly affected by the field flux. The two factors mentioned above vary depending on the material and shape of the core, but they must both be considered to obtain accurate leakage inductance values.

#### 4.1 Analysis of saturation

There is a region of the flux in the core that has more flux because the flux is flowing towards the smaller reluctance. As saturation is partially

different, saturation should be applied differently for each permeance. The saturation points are divided into the shoe, bend, and tooth parts. The bend of the bottom of the slot has high permeability in the yoke. thus, leakage rarely occurs. From the viewpoint of the leakage magnetic flux, if the core is saturated and the relative permeability is lowered, it can be regarded as an air-like substance. Therefore, it can be said that the effective width of the slot is relatively increased in the permeability calculation equation as it is saturated.

In this chapter, to consider only saturation by the armature current, the field current is set to 0 A. Figure 7 shows the relative permeability at three points according to the armature current. All the points are saturated when the current is 300 A, and the bend is the most saturated compared with the magnitude of the relative permeability. The bend region appears to be the most saturated due to the nature of the magnetic flux flowing into a small reluctance. Figure 8 shows the saturation of the bend. The saturation level is higher than those of the other parts because the magnetic flux flows much in the curved part, where the reluctance is small. A look at the rest of the points would reveal that the saturation level of the shoe was high at the low currents, but the saturation of the tooth was more severe than that of the shoe as the current increased.

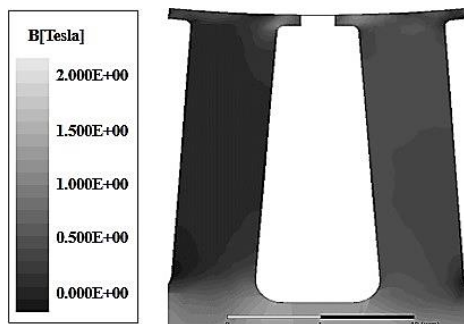


**Figure 8. Distribution of the saturation at the bend**

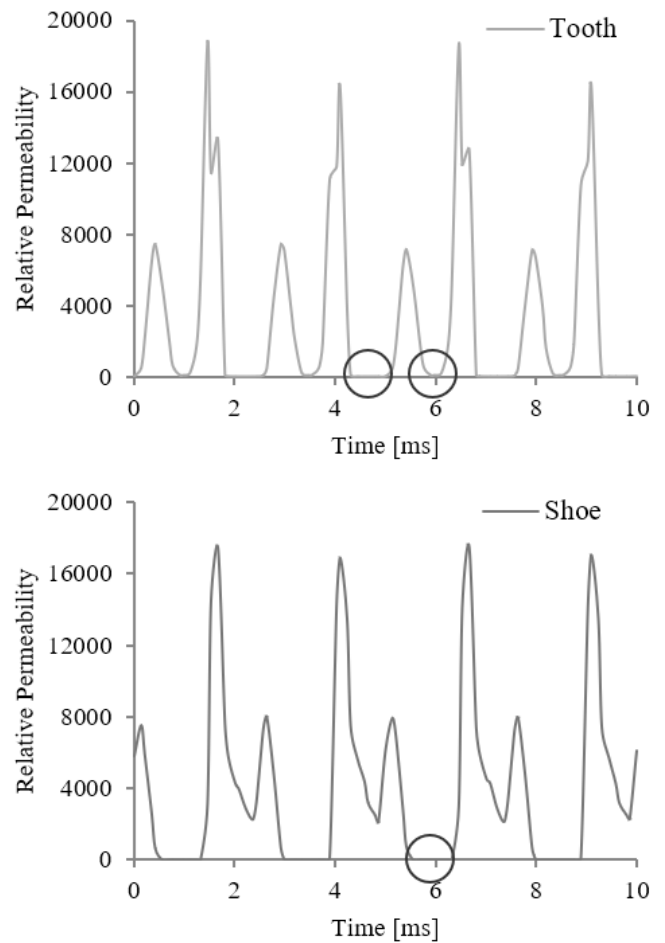


**Figure 9. Distribution of saturation when the current is 300A**

Figure 9 shows the distribution of the saturation when the current is 300 A. The areas marked with red circles are the saturation regions. When the current reaches the saturation spot, the saturation appears wider in the tooth than in the shoe. As the shoe is a small region, the above result is obtained because the area of saturation is smaller than that of the tooth even if the armature current increases. The overall saturation tendency is similar, but it is necessary to separate where the leakage flux is sensitive and where it is not. The formula for applying the rate of change of each part is as shown below.

$$L_s = N^2 \mu_0 L_{st} \left[ \frac{d_{r1}}{k_i w_{i1}} + \frac{d_{r2}}{k_i w_{i2}} + \frac{d_{i3}}{3k_i w_{i3}} + \frac{d_b}{k_b w_b} + \frac{d_s}{k_s w_s} \right] \quad (6)$$

In the above equation,  $k$  is a value obtained by calibrating the variation ratio of the relative permeability in Figure 7. The coefficient for saturation has a cumulative value. Therefore, the value for saturation converges towards the value of the point at which saturation occurs. Compared with the existing data, the graph results below are obtained.

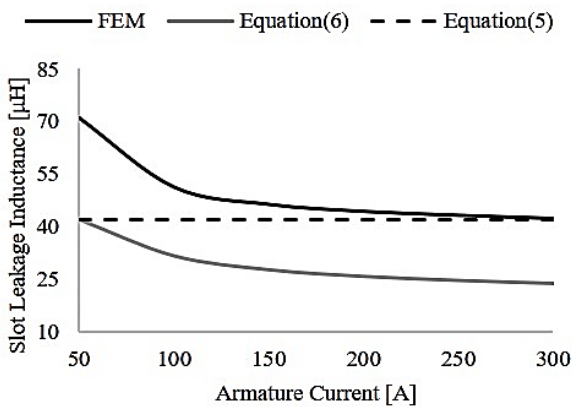


**Figure 10. Slot leakage inductance including the saturation coefficient**

**Table 3 : Slot leakage inductance values using different methods**

Ia	Slot leakage inductance						Unit
	50	100	150	200	250	300	A
FEM	71.0	51.3	46.4	44.4	43.3	42.4	μH
Eq(6)	42.0	31.6	27.6	25.7	24.5	23.7	
Eq(5)	42.04						

Figure 10 shows the slot leakage inductance including the saturation coefficient and value derived using the original equation. When the leakage inductance is calculated using the conventional formula, the saturation is not considered due to the current, and the inductance is constant even if the current changes. Table 3 shows data including the saturation coefficient. The magnitude of the leakage inductance is not correct, but the tendency is similar.

#### 4.2 Analysis of the field current

In addition to the magnetic flux generated by the armature current, the magnetic flux passing through the armature must be considered to obtain the accurate leakage magnetic flux. When the

field flux increases, the saturation phenomenon of the core should be considered.

**Table 4 : Slot leakage flux according to field and armature current**

If	Slot leakage flux						Unit
	Ia 50	100	150	200	250	300	A
6	2.88	4.66	6.56	8.54	10.5	12.3	mWb
9	3.20	4.88	6.74	8.69	10.7	12.6	
12	3.52	5.09	6.91	8.83	10.8	12.7	

Table 4 shows the change in the slot leakage magnetic flux according to the change in the field and armature currents. As the field current increases at the same armature current, the slot leakage flux steadily increases. As the armature current increases, saturation of the core occurs, and the change in the leakage flux decreases. In other words, the effect of saturation due to the increase in armature current is equally reflected in the field, and in the same armature current range, the magnetic flux due to the field current is almost constant. Therefore, the rate of change when the field current at the non-saturating point changes from 0 A to 12 A is digitized and substituted into the equation.

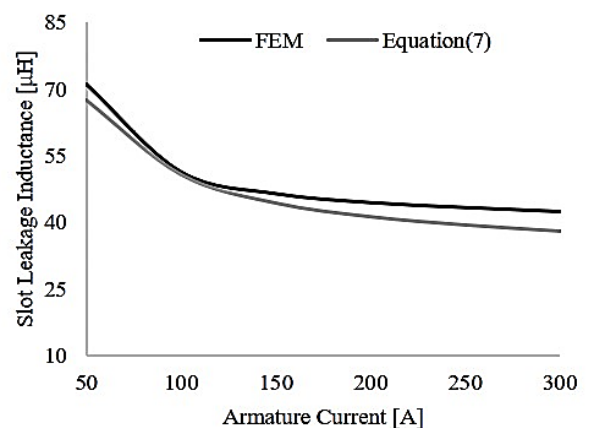


**Figure 11. Slot leakage inductance including saturation and field current**

If the coefficient for the change in the field flux is  $k_f$ , the new equation below is proposed considering the saturation and field current.

$$L_s = N^2 \mu_0 L_{si} k_f \left[ \frac{d_{t1}}{k_t w_{t1}} + \frac{d_{t2}}{k_t w_{t2}} + \frac{d_{t3}}{3k_t w_{t3}} + \frac{d_b}{k_b w_b} + \frac{d_s}{k_s w_s} \right] \quad (7)$$

Figure 11 shows the slot leakage inductance according to the change in the armature current when the field current is 12 A. Equation (7), which considers the field flux due to the saturation and field current, shows a graph similar to that of the measurement values obtained using FEM.

### 5. Conclusion

The calculation of the theoretical leakage inductance and measurement using the finite element method (FEM) have many errors. The main reason for this is that the formula does not take into account the nonlinear elements due to saturation, and does not reflect the field flux due to the field current. In this paper, FEM-based measurements and incorporation of the coefficients were compared to verify the effect of the saturation phenomenon and field flux on the leakage inductance. To precisely estimate the saturation phenomenon, the permeability was measured by dividing the slot of the FEM model into three parts that have a large influence on the leakage magnetic flux. In addition, the change in the leakage magnetic flux due to the field current was measured, digitized, and substituted into the formula. There were some errors due to the factors that were not considered, but it was proven that the measurement using FEM is similar to the formula using the coefficients.

### 6. Acknowledgment

This research was supported by the research fund of Hanbat National University in 2019.

### 7. References

- [1] Sung-In Park, Ki-Chan Kim. Torque Ripple Reduction Method with Asymmetric Pole for Wound-Field Synchronous Motor. *IEEE Trans. Mag*, March 2015, Vol. 51, No. 3
- [2] Sung-Woo Hwang, Jae-Han Sim, Jung-Pyo Hong and Ji-Young Lee. Torque Improvement of Wound Field Synchronous Motor for Electric Vehicle by PM-Assist. *IEEE Trans. Ind*, July-August 2018, Vol. 54, No. 4
- [3] Wenping Chai, Wenliang Zhao, and Byung-il Kwon. Optimal Design of Wound Field Synchronous Reluctance Machines to Improve Torque by Increasing the Saliency Ratio. *IEEE Trans. Mag*, November 2017, Vol. 53, No. 11
- [4] Myung-Seop Lim and Jung-Pyo Hong. Design of High Efficiency Wound Field Synchronous Machine with Winding Connection Change Method. *IEEE Trans, Energy conversion*, December 2018, Vol. 33, No. 4
- [5] Chang-Chou Hwang, Y. H. Cho. Effects of Leakage Flux on Magnetic Fields of Interior Permanent Magnet Synchronous Motors. *IEEE Trans. Mag*, July 2001, Vol. 37, No. 4
- [6] M. Faizul Momen, Susanta Datta. Analysis of Flux Leakage in a Segmented Core Brushless Permanent Magnet Motor. *IEEE Trans. Energy Conversion*, MARCH 2009, Vol. 24, No. 1
- [7] Alberto Tessarolo. Analytical Determination of Slot Leakage Field and Inductances of Electric Machines with Double-Layer Windings and semiclosed Slots. *IEEE Trans. Energy Conversion*, December 2015, Vol. 30, No. 4
- [8] K. Shima, K. Ide, M. Takahashi. Calculation of Leakage Inductances of a Salient-Pole Synchronous Machine Using Finite Elements. *IEEE Trans. Energy Conversion*, December 1999, Vol. 14, NO. 4
- [9] Ki-Chan Kim, Dong-Seok Ryu, and Min-Gyu Kim. Characteristics of Ferromagnetic Materials Due to Uneven Magnetic Saturation. *IEEE Trans. Mag*, October 2011, Vol. 47, NO. 10
- [10] Hyun-Soo Seol, Je-Myung Jeong, Ju Lee, and Chang-Sung Jin. Current Control of WRSM Considering Magnetic Saturation Phenomenon. *IEEE Trans. Mag*, July 2016, Vol. 52, No. 7

- [11] Ki-Chan Kim and Seung-Ha Jeon. Analysis on Correlation Between Cogging Torque and Torque Ripple by Considering Magnetic Saturation. IEEE Trans. Mag, May 2013, Vol. 49, No. 5
- [12] Duane Hanselman. Brushless Motors: Magnetic Design, Performance, and control. E-Man press LLC, 2012, pp. 63-114
- [13] Jacek F. Gieras. Electrical Machines. CRC Press Taylor & Francis Group, 2017, pp. 293-367